Spiral computed tomography evaluation of rabbit VX2 hepatic tumors treated with 20 kHz ultrasound and microbubbles

ZHI-YONG SHEN[1*], CHUN LIU[2*], MING-FENG WU[1], HAI-FENG SHI[1], YU-FENG ZHOU[1], WEI ZHUANG[1] and GAN-LIN XIA[1]

[1]Department of Radiology, Nantong Tumor Hospital, Nantong, Jiangsu 226361; [2]Laboratory Animal Center of Nantong University, Nantong, Jiangsu 226001, P.R. China

Received November 28, 2015; Accepted May 11, 2017

DOI: 10.3892/ol.2017.6557

Abstract. The aim of the present study was to explore the therapeutic effect of 20 kHz ultrasound (US) and microbubbles (MBs) on rabbit VX2 liver tumors by spiral computed tomography (CT) scanning. A total of 16 New Zealand rabbits with hepatic VX2 tumors were divided into four groups: Control, MB, low-frequency US and US + MB. The treatment effect was evaluated by spiral CT scanning prior to, during and following treatment (at 0 weeks and the end of 1 and 2 weeks). The tumor growth rate was recorded. The specimens of VX2 tumors were collected for histological examination and transmission electron microscopy (TEM). No significant differences were observed between tumor areas measured by CT and pathology after 2-week treatment (P>0.05). The mean tumor growth rates in the control, MB, US and US + MB groups after 2 weeks of treatment were 385±21, 353±12, 302±14 and 154±9%, respectively (P<0.05, US + MB vs. the other three groups). Hematoxylin and eosin staining in the US + MB group revealed coagulation necrosis, interstitial hemorrhage and intravascular thrombosis. In the control, MB and US groups, tumor cells exhibited clear nuclear hyperchromatism. TEM of US + MB revealed vascular endothelial cell wall rupture, widened endothelial cell gaps, interstitial erythrocyte leakage and microvascular thrombosis, while intact vascular endothelial cells and normal erythrocytes in the tumor vessels were observed in the control, MB and US groups. A combination of 20 kHz US and MBs may effectively inhibit rabbit VX2 tumors. Spiral CT scanning is an ideal method to evaluate the US treatment on rabbit tumors.

Correspondence to: Professor Gan-Lin Xia, Department of Radiology, Nantong Tumor Hospital, 30 North Tong-Yang Road, Nantong, Jiangsu 226361, P.R. China
E-mail: nt_radio@163.com

*Contributed equally

Key words: ultrasound, low-frequency, microbubble, cavitation, computed tomography, VX2 tumor

Introduction

Ultrasound (US) at 20 kHz is a special sound range just above the threshold of human hearing (1). The application of low-frequency (20 kHz) US has been demonstrated to be useful for increasing the efficiency and consumer safety in food processing (2), removing heavy metal (lead, mercury and arsenic) contamination in milk (3), decreasing the viscosity and particle size of milk (4) and improving the functional properties of dairy ingredients (5). US at a frequency of 20 kHz has been used to degrade the antibiotic ofloxacin in water (6). Low to moderate levels of ofloxacin degradation were reported, and this degradation was attributed to radical reactions in the liquid bulk rather than thermal reactions in the vicinity of the cavitation bubble (6).

US at 20 kHz can also increase membrane permeation (7). Size measurements and the direct visualization of vesicles demonstrate that US does not completely rupture membranes into fragments but causes transient poration, as leakage from the core is governed by acoustic cavitation (8). The extent of leakage inversely depends on the membrane thickness and directly depends on the sonication time and intensity (7).

US at 20 kHz is applied not only in industry but also to improve the *in vitro* and *in vivo* bio-effects in medicine (9-11). *In vitro* studies have demonstrated that 20 kHz US enhances the permeation of diclofenac sodium across EpiDerm™ 5-fold (9-11). It is a unique and exciting theranostic modality that can be used to track drug carriers, trigger drug release and improve drug deposition to tumor cells with high spatial precision (9). Cavitation bubbles induced by 20 kHz US may induce cell death or transient membrane permeabilization, which is defined as sonoporation on a single cell level (10). Microscopy disclosed that the collapse of a microbubble (MB) and generation of a jet produce small holes within cell membranes (12). Pores produced within the cell membrane may be transient (facilitating successful therapeutic delivery) or permanent (resulting in cell death) (13). The application of sonoporation can be used to deliver genes into cells (14,15). *In vitro*, a variety of cell lines, including fibroblast cells, ovarian carcinoma cells and HeLa cells, have been successfully transfected for gene therapy (14-16) with concomitant cell death (17).

In vivo studies demonstrated a loss of balance stability and reduced motor response time in humans due to 20 kHz

airborne US up to 1 h with 120 dB (18) and temporary hearing loss for 5 min at 154 dB (19). Human subjects complained of fatigue, headache, nausea and tinnitus as a result of the airborne ultrasonic exposure at 20 kHz and 110 dB for 1 day (20). Nude mice succumbed after 8-70 min of exposing the head to 20 kHz with a sound pressure of 162 dB (21). Boucaud *et al* (22) researched the human skin bio-effect of a 20-kHz contact US pulse wave with a 10% duty cycle (0.1 sec on, 0.9 sec off) and a 20-kHz continuous wave for 10 min with a varying intensity of 0.25-7 W/cm^2. They found that 20 kHz US significantly increased skin permeabilization. The skin permeabilization induced by 20 kHz US results primarily from the direct mechanical impact of gas bubbles that collapse on the skin surface (resulting in microjets and shockwaves) (22). Tang *et al* (23) studied pig skin permeabilization effects of a coupling medium with 20 kHz US, with a 10% duty cycle (0.1 sec on, 0.9 sec off) for 2 h at a power of 1.6-33.5 W/cm^2. The results indicated that US-induced cavitation in the coupling medium is the key mechanism of skin permeabilization during low frequency sonophoresis. Transient cavitation occurring on, or in the vicinity of, the skin membrane is the central mechanism responsible for the observed enhancement of skin permeability (23).

The industrial and medical applications of 20 kHz US are diverse, ranging from high power industrial US equipment to various therapeutic medical applications (24,25). Previous studies have investigated the effects of low-frequency US on small animals, including nude mice, and revealed that low-frequency US could downregulate the expression of vascular-related protein (25) and inhibit tumor growth (26). However, the cavitation effect on tumors in larger animals, including rabbits, has not been thoroughly studied. When MBs are intravenously injected, the acoustic pressures that facilitate the therapeutic effects will decrease (27). Thus, the present study aimed to explore the effects of 20 kHz US and MBs on rabbit liver tumors using computed tomography (CT) and compare them with pathology as a reference standard.

Materials and methods

Animal protocol and tumor inoculation. The experiments were performed with 16 New Zealand white rabbits that weighed 2.0-2.5 kg (median, 2.2 kg). All 16 rabbits were male, aged 90 days and were provided from the Laboratory Animal Center of Nantong University (Nantong, China). The experiments were approved by the Animal Care Committee of Nantong University Medical School (Jiangsu, China) and were performed in accordance with the institutional guidelines. The animals were anesthetized with an intravenous injection of 30 mg/kg pentobarbital. VX2 carcinoma cells (Department of Ultrasound in Medicine, Shanghai Jiao Tong University Affiliated Sixth People's Hospital, Shanghai, China) were used to establish a model of hepatic tumors. The abdomens of the recipient rabbits were shaved and prepared with povidone iodine, and a midline subxyphoid incision was made. The anterior surface of the liver was exposed, and prepared tumor tissue was implanted in the liver lobe using forceps. The outlet of the inoculated area was blocked by a gelatin sponge (Suzhong Medical Instrument Co., Ltd., Yangzhou, Jangsu, China). Only one inoculation site was used per liver. Aseptic technique was maintained during each inoculation. Following surgery, the animals were returned to their cages, kept warm (temperature 18˚C; humidity, 65%; good ventilation; dim light; quiet environment; and with sufficient food and clean water) and monitored in the animal laboratory until they recovered from anesthesia. An iU22 ultrasound system (Philips Medical Systems, Inc., Bothell, WA, USA) with a 12-15 MHz broadband linear probe was used to monitor the tumor growth every day following tumor inoculation. VX2 carcinoma nodules reaching 0.8-0.9 cm in diameter were considered appropriate for low-frequency US treatment. The period for tumors to reach a size of 0.8 cm ranged from 12 to 13 days. The same investigator performed all inoculations and inoculated specimens of the same tumor into all rabbits to minimize inter-animal variations in the tumor growth rate.

Experimental protocol. In the present study, 16 tumor-bearing rabbits were randomly divided into four groups, with 4 rabbits per group: Group A, negative control (sham treatment); group B, MB; group C, low-frequency US; and group D, US + MB. The MBs used were an US contrast agent (SonoVue; Bracco SpA, Milan, Italy). The rabbits were anesthetized via an auricular vein injection of 30 mg/kg pentobarbital, which is a routine site for vein injection in rabbits (28).

Subsequent to successful anesthesia, an iU22 ultrasound system (Philips Medical Systems, Inc.) was used to locate the liver tumor prior to insonication. The hepatic tumors were subsequently sonicated using a focused low-frequency US transducer manufactured by Taizhou Research Institute of Ultrasound Technology (Taizhou, Jiangsu, China). The probe was placed on the shaved abdominal skin of rabbits covered with a US transmission gel (a Lotus medical ultrasonic coupling agent; Yi Jie Guangzhou Pharmaceutical Technology Co., Ltd., Guangzhou, China) to ensure US propagation. The diameter of the therapeutic US transducer was ~24 mm. The low-frequency US parameters were set to 20 kHz, 2 W/cm^2, duty cycle 40% (on 2 sec, off 3 sec) and a duration of 5 min once every other day for 2 weeks. The US contrast agent was simultaneously and continuously infused with US wave irradiation via the auricular vein of rabbits (at a flow rate of 0.2 ml/min). The dose of the contrast agent administered was 1 ml (0.4 ml/kg) per rabbit for each treatment. The concentration of the contrast agent was 1.8x10^9 MBs/ml.

CT scanning. The rabbits were fasted for 8 h before scanning and anesthetized with an intramuscular injection of 0.2 ml/kg sumianxin (1 ml, including 4 μg dihydroetorphine and 2.5 mg aloperidin; Nantong University Animal Center, Nantong, China). CT perfusion scans were performed before and at 1 and 2 weeks after tumor treatment. CT imaging was completed on a multi-slice spiral CT (LightSpeed 16-Slice Spiral CT; GE Healthcare, Chicago, IL, USA). To select the scanning range, a plain CT scan of the liver was performed prior to beginning perfusion scanning. The CT scanning parameters were defined as follows: 80 kVp; 120 mAs; slice thickness, 3 mm; matrix, 512x512; field of view, 15 cm; and contrast medium IV injection in marginal ear vein, 1 ml/sec (1.0-1.5 ml/kg body weight). The tumor size on imaging studies was recorded as the median of the maximum transverse and anteroposterior dimensions. Following treatment, the tumor

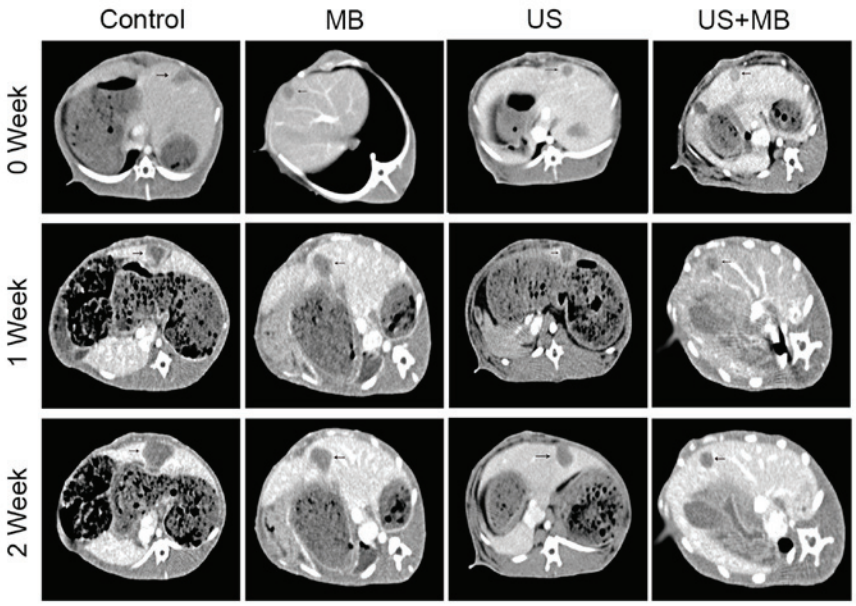

Figure 1. Representative computed tomography images of tumors (arrows) prior to and following treatment in the control, MB, US and US + MB groups. US, ultrasound; MB, microbubble.

area was determined each week by measuring the transversal and anteroposterior tumor diameters. The tumor growth rate (%) = (transversal x anteroposterior diameters) after therapy - (transversal x anteroposterior diameters) before therapy/(transversal x anteroposterior diameters) before therapy x100.

Histological examination. At the end of the therapy experiment, 16 rabbits with 4 rabbits per group were sacrificed by established technique, and the maximum cross-section areas of the hepatic tumors were calculated based on the anatomical measurements and compared with the CT results. The tumor specimens were then collected and cut into two sections for histological examination (thickness, 1 cm) and transmission electron microscopy (TEM; thickness, 1 mm). The tumor tissues intended for histology examination were fixed with 10% neutral formaldehyde solution for 24 h at 18˚C and embedded in paraffin, and each tumor was stained using hematoxylin and eosin (H&E) for 2 h at 18˚C. Subsequently, the structure of the tumor cells was observed using an Olympus microscope (BX50; magnification, x200; Olympus Corporation, Tokyo, Japan). A histopathologist blind to the study evaluated the findings using microscopy.

TEM. Each tumor sample intended for TEM was ~1 mm^3 in volume and fixed in 2% glutaraldehyde and PBS for 2 h at 4˚C, followed by two washes in PBS buffer for 10 min. Following treatment with 1% osmium tetroxide in PBS, the specimens were fixed with 1% osmic acid at 4˚C for 2 h and dehydrated via immersion in 30% ethanol, followed by 50 and 70% ethanol three times each for 10 min. The samples were then embedded in propylene oxide at 18˚C for 2 h and stained with lead citrate E for 12 h at 18˚C. Finally, the specimens were examined after sectioning using TEM (Philips CM-120; Philips Molecular Systems, Inc.).

Statistical analysis. The data were presented as median ± standard deviation. Statistical analysis was performed using SPSS version 11.0 (SPSS, Inc., Chicago, IL, USA). The tumor sizes were subjected to Student's t-test to statistically compare groups. Multiple groups were compared using a one-way analysis of variance (ANOVA), and the two groups were compared using the Newman-Keuls test. $P<0.05$ was considered to indicate a statistically significant difference.

Results

Comparison of CT and pathology measurements. The CT images of 16 hepatic tumors in rabbits were obtained (Fig. 1). A basic rabbit liver scan showed a low density of tumors, while the tumors were markedly enhanced in the arterial phase, with no enhancement in the necrotic tissue within the tumor and in the surrounding normal liver parenchyma, which manifested a clear demarcation. The portal venous phase scan indicated a low density of tumors and clear enhancement of the surrounding normal liver parenchyma, which best clarified the tumor margins (Fig. 1). The tumor size and area calculated based on CT data and pathology measurements did not significantly differ at 2 weeks ($P>0.05$; Table I).

Tumor growth result with CT. As shown in Table II, the calculation of tumor size of the maximum transverse and anteroposterior dimensions. The tumor growth rates at 1 and 2 weeks based on CT are also shown in Table II and Fig. 2. The mean tumor growth rates after 2 weeks in the control, MB, US and US + MB groups were 385±21, 353±12, 302±14 and 154±9%, respectively. The tumor growth rate significantly differed among the four groups and was determined using the ANOVA test, with $F=87.53$ and $P<0.0001$. A Newman-Keuls multiple comparison test identified a significant difference between the US + MB group and the other three groups

Table I. Comparison of tumor area on CT and pathology after 2 weeks.

Group	CT (D1 x D2), mm	Anatomy (D1 x D2), mm	t value	P-value
Control	22±2.2x21±1.8	20±1.6x21±1.6	-0.03	0.9782
MB	19±2.2x18±2.4	19±1.4x19±1.8	-0.66	0.5763
US	18±2.2x17±2.6	18±2.3x18±2.4	-1.87	0.1579
US + MB	14±2.3x14±2.2	15±1.4x15±1.4	1.27	0.2936

Data are presented as the median ± standard deviation. D1, transversal diameter of the tumor; D2, anteroposterior diameter of the tumor; MB, microbubble; US, ultrasound; CT, computed tomography.

Table II. Growth rate of rabbit hepatic tumor area calculated by computed tomography in the four groups.

Groups	Pre (D1 x D2), mm	1 week (D1 x D2), mm	2 week (D1 x D2), mm	GR 1 week, %	GR 2 weeks, %
Control	9±0.1x9±0.1	13±1.2x13±2.3	22±2.2x21±1.8	101±9	385±21
MB	9±0.2x8±0.1	12±2.3x12±1.4	19±2.2x18±2.4	92±6	353±12
US	9±0.1x8±0.2	11±2.1x12±2.4	18±2.2x17±2.6	77±4	302±14
US + MB	9±0.2x8±0.1	11±2.2x11±1.8	14±2.3x14±2.2	73±6	154±9

Data are presented as the median ± standard deviation. D1, transversal diameter of the tumor; D2, anteroposterior diameter of the tumor; Pre, pre-treatment; GR, growth rate following treatment; MB, microbubble; US, ultrasound.

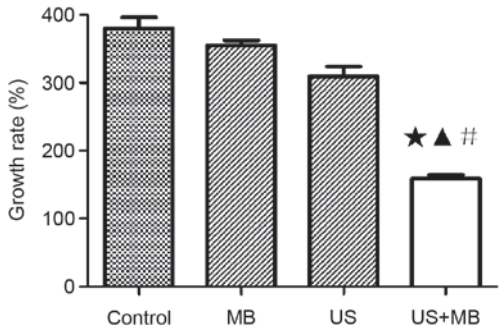

Figure 2. Tumor growth rate of each group in computed tomography. The growth rate significantly differed between the US + MB group and the other three groups ★P<0.05 vs. control; ▲P<0.05 vs. MB; #P<0.05 vs. US. US, ultrasound; MB, microbubble.

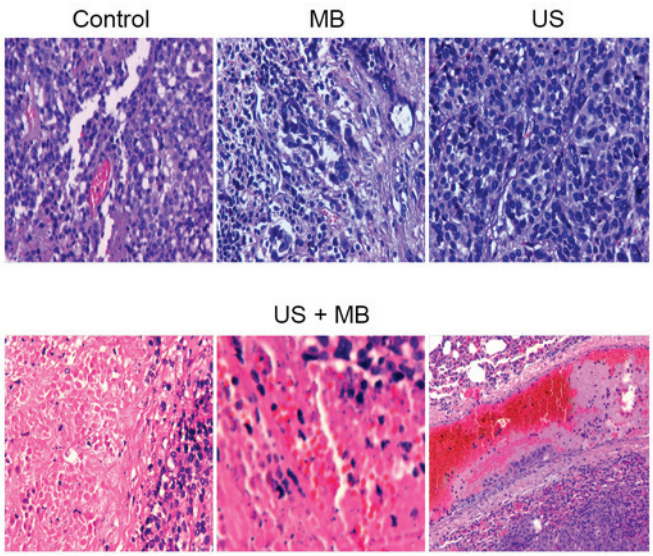

Figure 3. H&E staining results for the control, MB, US and US + MB groups (magnification, x200). Intact live tumor tissues in the control, MB and US groups grew in as solid pattern without clear vascular rupture and necrosis. However, the H&E staining in the US + MB group revealed coagulation necrosis, hemorrhage in the tumor tissue and thrombogenesis in the vessels. H&E, hematoxylin and eosin; MB, microbubble; US, ultrasound.

(P<0.05), but the control, MB and US groups did not significantly differ (P>0.05) (Table II and Fig. 2). The mean tumor growth rates in the control, MB, US and US + MB groups after 1 week of treatment were 101±9, 92±6, 77±4 and 73±6%, respectively. The tumor growth rate did not significantly differ between the US + MB group and the other three groups after 1 week (P>0.05; Table II).

Histological findings. The US + MB group showed tumor coagulation necrosis (magnification, x200). Diffused interstitial hemorrhage and vascular thrombus were also observed 2 weeks after treatment. Residual liver neoplastic cells could be found only at the peripheral border area. In the control, MB and US groups, intact liver tumor tissues grew in a solid pattern without evident vascular rupture and necrosis (Fig. 3).

TEM results. TEM revealed vascular endothelial cell wall rupture, widened endothelial cell gaps, interstitial erythrocyte leakage and vascular lumen thrombosis in the US + MB group. The majority of tumor cells in the other three groups appeared normal. Intact vascular lumen and normal erythrocytes in the tumor vessels were observed in the control, MB and US groups (Fig. 4).

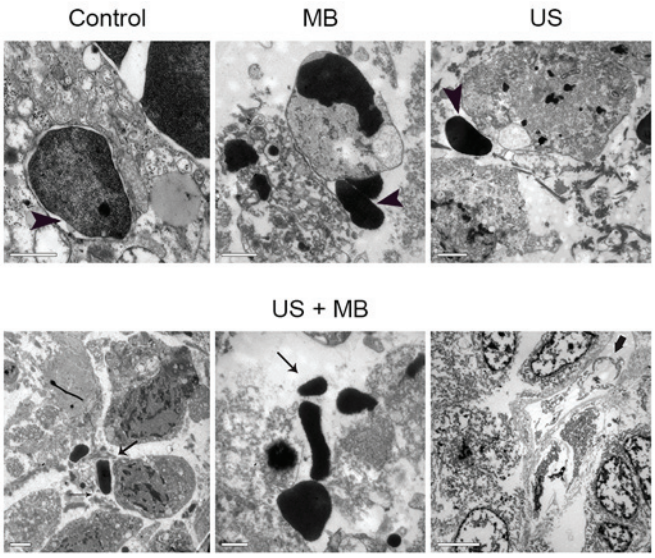

Figure 4. Microvessels of transmission electron microscopy in the control (scale bar, 1 μm), MB (scale bar, 1 μm) and US (scale bar, 2 μm) groups had an intact vascular lumen and normal erythrocytes in the vessels (arrow head); ruptured vascular endothelial cells (scale bar, 2 μm), a widened endothelial cell gap (scale bar, 2 μm) (slim arrow), erythrocyte exudation (scale bar, 1 μm) (slim arrow) and microvascular thrombosis (scale bar, 5 μm) (wider arrow) were observed in the US + MB group.

Discussion

The present study did not indicate significant differences between the tumor area calculated based on CT and pathology data after 2 weeks of treatment in the four groups, with P>0.05 in all cases. CT is an accurate method to evaluate the curative effect of liver cancer treatments (29). Enhanced CT can accurately detect the tumor vasculature. It detected not only the border of the tumors but also internal necrosis due to the non-enhancement of the tumors. Thus, CT is a useful tool to evaluate liver cancer therapy and tumor necrosis, and to measure the exact area of a tumor.

The present study used 20 kHz US, which is the lowest frequency point on the US wave (30). This frequency was selected as higher sound frequencies accelerate the vibration of the MB in the sound field while reducing the amplitude (31). The time interval of the sonic pressure half cycle between the acoustic positive and negative range is short, which decreased the expansion of MBs; the attraction between the liquid molecules is not easily broken, which hinders the formation of a cavitation bubble (31). Therefore, high frequency US requires higher sound pressures to generate cavitation nuclei. The intensity threshold of collapse cavitation positively correlates with the frequency of US (32). The onset of collapse cavitation at 20 kHz occurs at ~0.015 W/cm^2, while this threshold increases to 0.38 W/cm^2 at 70 kHz (33). By contrast, when MB was irradiated with lower frequency US, such as 20 kHz, the amplitude of MB increased (25). The vibration time at negative pressure is longer; thus, the liquid-phase intermolecular attraction breaks more easily and more cavitation nuclei form (34). Furthermore, the longer time gap between the compression and expansion of the liquid affords the cavitation bubble with more time to grow prior to bursting, and the volume of the cavitation bubble is positively associated with the intensity of the cavitation effects when the bubble collapses (35). Thus, selecting an appropriate ultrasonic frequency is crucial to the induced cavitation effect.

The present study revealed that the tumor growth rate in the US + MB group was lower than those in the control, MB and US groups. In addition, vascularization damage was another important result. The tumor cannot grow without angiogenesis and malignant tumors are always rich in vasculature (36). The present results demonstrated that the vascularization of rabbit liver tumors significantly changed in the US + MB group compared with the other three groups. H&E staining revealed tumor microvascular internal thrombosis in certain areas, the interstitial exudation of red blood cell (RBC) and tumor cell necrosis. US combined with MBs can effectively destroy the tumor blood vessels and inhibit the growth of the tumor (26). Previous studies have reported that MB destruction during US exposure ruptures microvessels and causes RBCs to extravasate (37,38).

TEM in the present study revealed tumor capillary vessel wall fracture, cavity thrombosis and interstitial exudation of RBCs in the US + MB group, and these findings were consistent with the results of the H&E staining. US combined with MBs caused significant vascular changes, which may be due to the following. Sonovue, a second-generation contrast agent, is a phospholipid coated, sulfur hexafluoride gas-containing MB, whose diameter is much smaller than that of room air-filled bubbles (~2.5 mm) (39). This smaller diameter improves the passage into the pulmonary capillary bed and allows the bubbles to reach the micro-circulation of rabbit hepatic tumors (39). MBs expand and contract in size in response to the oscillating pressure and energy accumulates when the MBs are constricted by sound pressure (40). Ultimately, the energy carried by cavitation bubbles is released when the MBs collapse and sonication cavitation occurs and during the cavitation, the MBs undergo volumetric oscillations, thereby changing the local mechanical condition of the tissue (40). When MBs collapse, they can create shockwaves, increasing the local pressure by 100 atm and the local temperature by several thousands of degrees (41). Shockwaves can cause substantial cell damage and possible cell lysis nearby (42). The destruction of MBs may cause high-energy microstreams or microjets that will result in shear stress on the membrane of an endothelial cell and increase its permeability (43).

During US sonication in the presence of MBs, the oscillation, collapse and cavitation of MBs in the acoustic beam produced vascular pores and disrupted the vessel wall to significantly increase the vascular permeability in the sonicated areas (35). This process may have led to the formation of smaller bubbles, which interacted with the US beam and caused the cellular bio-effects (44).

Other bio-effects include the free radicals generated during MB collapse (41). The formation of highly reactive species, including OH, H, HO_2 and H_2O_2, due to the transient collapse of cavitation bubbles is the primary mechanism of the sonochemical reaction (41), which can also damage the vessel wall.

Notably, microvessel rupture was not observed in response to US exposure. Similarly, ruptures were also absent when MBs were infused in the absence of US. When MB infusion and US exposure were performed simultaneously, the destruction of MBs was evident in the microvessels of rabbit hepatic

tumors. The cumulative effects of 2 weeks of US sonication may have ruptured tumor vessels and induced hemorrhage, which would have destroyed the normal structural support for the capillaries. In general, tumor vascular rupture, interstitial erythrocyte leakage and continual injury induced by MB cavitation result in tumor ischemia, which may explain the tumor growth inhibition in the MB + US group ($P<0.05$ compared with the other three groups), as presented in Fig. 2.

However, the disruption of blood vessels in the sonicated tumors can enhance tumor inhibition, while it may also facilitate the intravasation of tumor cells into circulation to increase metastasis. Future studies should investigate the possibility of metastasis increase in response to MB + US treatment.

Acknowledgements

The present study was supported in part by the Nantong Municipal Science and Technology Project (grant no. MS12016033 and HS149072), the Nantong Municipal Youth Fund Project (grant no. WQ2015054) and the Six Talent Peaks Project in Jiangsu Province (grant no. WSW-081).

References

1. Fausti SA, Erickson DA, Frey RH, Rappaport BZ and Schechter MA: The effects of noise upon human hearing sensitivity from 8000 to 20 000 Hz. J Acoust Soc Am 69: 1343-1347, 1981.
2. Miano AC, Ibarz A and Augusto PE: Mechanisms for improving mass transfer in food with ultrasound technology: Describing the phenomena in two model cases. Ultrason Sonochem 29: 413-419, 2016.
3. Porova N, Botvinnikova V, Krasulya O, Cherepanov P and Potoroko I: Effect of ultrasonic treatment on heavy metal decontamination in milk. Ultrason Sonochem 21: 2107-2111, 2014.
4. Gao S, Hemar Y, Lewis GD and Ashokkumar M: Inactivation of enterobacter aerogenes in reconstituted skim milk by high- and low-frequency ultrasound. Ultrason Sonochem 21: 2099-2106, 2014.
5. Zisu B, Bhaskaracharya R, Kentish S and Ashokkumar M: Ultrasonic processing of dairy systems in large scale reactors. Ultrason Sonochem 17: 1075-1081, 2010.
6. Hapeshi E, Achilleos A, Papaioannou A, Valanidou L, Xekoukoulotakis NP, Mantzavinos D and Fatta-Kassinos D: Sonochemical degradation of ofloxacin in aqueous solutions. Water Sci Technol 61: 3141-3146, 2010.
7. Pangu GD, Davis KP, Bates FS and Hammer DA: Ultrasonically induced release from nanosized polymer vesicles. Macromol Biosci 10: 546-554, 2010.
8. Fu H, Comer J, Cai W, Cai W and Chipot C: Sonoporation at small and large length scales: Effect of cavitation bubble collapse on membranes. J Phys Chem Lett 6: 413-418, 2015.
9. Sirsi SR and Borden MA: State-of-the-art materials for ultrasound-triggered drug delivery. Adv Drug Deliv Rev 72: 3-14, 2014.
10. Forbes MM, Steinberg RL and O'Brien WD Jr: Frequency-dependent evaluation of the role of definity in producing sonoporation of Chinese hamster ovary cells. J Ultrasound Med 30: 61-69, 2011.
11. Aldwaikat M and Alarjah M: Investigating the sonophoresis effect on the permeation of diclofenac sodium using 3D skin equivalent. Ultrason Sonochem 22: 580-587, 2015.
12. Ohl CD, Arora M, Ikink R, de Jong N, Versluis M, Delius M and Lohse D: Sonoporation from jetting cavitation bubbles. Biophys J 91: 4285-4295, 2006.
13. Ward M, Wu J and Chiu JF: Ultrasound-induced cell lysis and sonoporation enhanced by contrast agents. J Acoust Soc Am 105: 2951-2957, 1999.
14. Domenici F, Giliberti C, Bedini A, Palomba R, Luongo F, Sennato S, Olmati C, Pozzi D, Morrone S, Congiu Castellano A and Bordi F: Ultrasound well below the intensity threshold of cavitation can promote efficient uptake of small drug model molecules in fibroblast cells. Drug Deliv 20: 285-295, 2013.
15. Florinas S, Kim J, Nam K, Janát-Amsbury MM and Kim SW: Ultrasound-assisted siRNA delivery via arginine-grafted bioreducible polymer and microbubbles targeting VEGF for ovarian cancer treatment. J Control Release 183: 1-8, 2014.
16. Javadi M, Pitt WG, Tracy CM, Barrow JR, Willardson BM, Hartley JM and Tsosie NH: Ultrasonic gene and drug delivery using eLiposomes. J Control Release 167: 92-100, 2013.
17. Miller DL, Pislaru SV and Greenleaf JE: Sonoporation: Mechanical DNA delivery by ultrasonic cavitation. Somat Cell Mol Genet 27: 115-134, 2002.
18. Dobroserdov VK: On the effect of low frequency ultrasonic waves and high frequency sound waves on the organism of workers. Gig Sanit 32: 17-21, 1967 (In Russian).
19. Davis H, Parrack HO and Eldredge DH: Hazards of intense sound and ultrasound. Ann Otol Rhinol Laryngol 58: 732-738, 1949.
20. Acton WI and Carson MB: Auditory and subjective effects of airborne noise from industrial ultrasonic sources. Br J Ind Med 24: 297-304, 1967.
21. Acton WI: The effects of industrial airborne ultrasound on humans. Ultrasonics 12: 124-128, 1974.
22. Boucaud A, Montharu J, Machet L, Arbeille B, Machet MC, Patat F and Vaillant L: Clinical, histologic and electron microscopy study of skin exposed to low-frequency ultrasound. Anat Rec 264: 114-119, 2001.
23. Tang H, Wang CC, Blankschtein D and Langer R: An investigation of the role of cavitation in low-frequency ultrasound-mediated transdermal drug transport. Pharm Res 19: 1160-1169, 2002.
24. Mawson R, Rout M, Ripoll G, Swiergon P, Singh T, Knoerzer K and Juliano P: Production of particulates from transducer erosion: Implications on food safety. Ultrason Sonochem 21: 2122-2130, 2014.
25. Shen ZY, Shen E, Zhang JZ, Bai WK, Wang Y, Yang SL, Nan SL, Lin YD, Li Y and Hu B: Effects of low-frequency ultrasound and microbubbles on angiogenesis-associated proteins in subcutaneous tumors of nude mice. Oncol Rep 30: 842-850, 2013.
26. Shen ZY, Shen E, Diao XH, Bai WK, Zeng MX, Luan YY, Nan SL, Lin YD, Wei C, Chen L, *et al*: Inhibitory effects of subcutaneous tumors in nude mice mediated by low-frequency ultrasound and microbubbles. Oncol Lett 7: 1385-1390, 2014.
27. Ferrara KW: Driving delivery vehicles with ultrasound. Adv Drug Deliv Rev 60: 1097-1102, 2008.
28. Shen ZY, Xia GL, Wu MF, Ji LY and Li YJ: The effects of percutaneous ethanol injection followed by 20-kHz ultrasound and microbubbles on rabbit hepatic tumors. J Cancer Res Clin Oncol 142: 373-378, 2016.
29. Chen G, Ma DQ, He W, Zhang BF and Zhao LQ: Computed tomography perfusion in evaluating the therapeutic effect of transarterial chemoembolization for hepatocellular carcinoma. World J Gastroenterol 14: 5738-5743, 2008.
30. Ohl SW, Klaseboer E and Khoo BC: Bubbles with shock waves and ultrasound: A review. Interface Focus 5: 20150019, 2015.
31. Izadifar Z, Babyn P and Chapman D: Mechanical and biological effects of ultrasound: A review of present knowledge. Ultrasound Med Biol 43: 1085-1104, 2017.
32. Vlaisavljevich E, Lin KW, Warnez MT, Singh R, Mancia L, Putnam AJ, Johnsen E, Cain C and Xu Z: Effects of tissue stiffness, ultrasound frequency and pressure on histotripsy-induced cavitation bubble behavior. Phys Med Biol 60: 2271-2292, 2015.
33. Husseini GA, Abdel-Jabbar NM, Mjalli FS and Pitt WG: Modeling and sensitivity analysis of acoustic release of doxorubicin from unstabilized pluronic P105 using an artificial neural network model. Technol Cancer Res Treat 6: 49-56, 2007.
34. Shneidman VA: Time-dependent cavitation in a viscous fluid. Phys Rev E 94: 062101, 2016.
35. Shen ZY, Xia GL, Wu MF, Shi MX, Qiang FL, Shen E and Hu B: The effects of low-frequency ultrasound and microbubbles on rabbit hepatic tumors. Exp Biol Med (Maywood) 239: 747-757, 2014.
36. Verdelli C, Avagliano L, Creo P, Guarnieri V, Scillitani A, Vicentini L, Steffano GB, Beretta E, Soldati L, Costa E, *et al*: Tumour-associated fibroblasts contribute to neoangiogenesis in human parathyroid neoplasia. Endocr Relat Cancer 22: 87-98, 2015.
37. Skyba DM, Price RJ, Linka AZ, Skalak TC and Kaul S: Direct in vivo visualization of intravascular destruction of microbubbles by ultrasound and its local effects on tissue. Circulation 98: 290-293, 1998.
38. Price RJ, Skyba DM, Kaul S and Skalak TC: Delivery of colloidal particles and red blood cells to tissue through microvessel ruptures created by targeted microbubble destruction with ultrasound. Circulation 98: 1264-1267, 1998.

39. Liu Y, Ren W, Liu C, Huang K, Feng Y, Wang X and Tong Y: Contrast-enhanced ultrasonography of the rabbit VX2 tumor model: Analysis of vascular pathology. Oncol Lett 4: 685-690, 2012.
40. Kollath A, Brezhneva N, Skorb EV and Andreeva DV: Microbubbles trigger oscillation of crystal size in solids. Phys Chem Chem Phys 19: 6286-6291, 2017.
41. Merouani S, Hamdaoui O, Rezgui Y and Guemini M: Theoretical estimation of the temperature and pressure within collapsing acoustical bubbles. Ultrason Sonochem 21: 53-59, 2014.
42. Coralic V and Colonius T: Shock-induced collapse of a bubble inside a deformable vessel. Eur J Mech B Fluids 40: 64-74, 2013.
43. Suzuki R, Oda Y, Utoguchi N and Maruyama K: Progress in the development of ultrasound-mediated gene delivery systems utilizing nano- and microbubbles. J Control Release 149: 36-41, 2011.
44. Lin CY, Tseng HC, Shiu HR, Wu MF, Chou CY and Lin WL: Ultrasound sonication with microbubbles disrupts blood vessels and enhances tumor treatments of anticancer nanodrug. Int J Nanomedicine 7: 2143-2152, 2012.